Applied Catalysis A: General 443–444 (2012) 40–49

Contents lists available at SciVerse ScienceDirect

Applied Catalysis A: General

journal homepage: www.elsevier.com/locate/apcata

Total oxidation of model volatile organic compounds over some commercial catalysts

Lenka Matějová, Pavel Topka*, Květuše Jirátová, Olga Šolcová

Institute of Chemical Process Fundamentals of the ASCR, v. v. i., Rozvojová 135, CZ-165 02 Praha 6, Czech Republic

ARTICLE INFO

Article history:
Received 17 February 2012
Received in revised form 13 July 2012
Accepted 16 July 2012
Available online 22 July 2012

Keywords:
Oxidation
Volatile organic compounds
Ethanol
Toluene
Dichloromethane

ABSTRACT

Commercial VOC oxidation catalysts can be used as comparative materials during development of new or improved catalysts. The objective of this study was to investigate physicochemical properties of EnviCat® commercial catalysts and their performance in total oxidation of three model compounds (dichloromethane, toluene and ethanol) at laboratory scale. The reactivity of model VOC was decreasing in the order ethanol > toluene > dichloromethane. The Cu–Mn/Al catalyst was found to be the most active and selective catalyst in ethanol oxidation. In oxidation of dichloromethane, the Pt–Pd/Al–Ce catalyst with 0.10 wt% Pt + Pd was the most active, while the most selective one (giving the highest HCl yield) was the Pt–Pd/Al catalyst containing 0.24 wt% Pt + Pd. In toluene oxidation, the Pt–Pd/Al catalyst with 0.24 wt% Pt + Pd possessed the highest activity; the selectivity to CO_2 was 100% for all investigated catalysts. Obtained results showed that the performance of commercial catalysts in laboratory scale tests can be different from that declared by catalyst supplier. A possible difference in catalytic performance at industrial and laboratory scale should be taken into account when industrial catalysts are used in laboratory scale tests.

© 2012 Elsevier B.V. All rights reserved.

1. Introduction

Volatile organic compounds (VOC) are known as one of the major contributors to air pollution. They may have short and long-term adverse health effects, act as greenhouse gases and are the major source of ground-level ozone, which is the primary constituent of the photochemical smog [1,2]. Anthropogenic sources of VOC include chemical plants, petroleum refineries, power plants, gas stations and dry cleaners. Moreover, an increasing amount of carcinogenic VOC like formaldehyde and acetaldehyde is produced due to growing utilization of the ethanol-based biofuels in cars [3].

The VOC emissions are regulated by the legislation of European Union since 1999, when the Solvent Directive was launched. In 2005, the Commission of the European Communities published the Thematic Strategy on Air Pollution [4]. Its aim is to cut the annual number of premature deaths caused by air pollution by 40% of the 2000 level in 2020 and to reduce the continuing damage to Europe's ecosystems. In order to achieve these aims, the emissions of VOC will need to be reduced by 51% compared to their 2000 levels.

Oxidation is the most commonly used technique for VOC control. Typically, VOCs have been removed using thermal incineration at temperatures higher than 900 °C. However, the thermal decomposition is gradually being replaced by catalytic oxidation, which can be carried out at lower temperatures (below 500 °C) and is therefore regarded as efficient, cost-effective and environmentally friendly way to treat VOC emissions [5]. Moreover, the lower temperature and the use of appropriate catalyst avoid generation of dangerous reaction by-products like NO_x [6].

The most commonly used VOC oxidation catalysts are based on supported noble metals or transition metal oxides. Metal oxides, mainly of Co, Cu, Ni and Mn, have the advantage of having lower cost and greater resistance to deactivation by poisoning [7]. On the other hand, noble metal catalysts are generally preferred because of their high activity, excellent stability and good selectivity to CO_2 [8]. Both types of catalysts have been extensively studied in the literature [9,10].

Commercial VOC oxidation catalysts may be used as the comparative catalytic materials during catalytic testing of newly developed catalysts at laboratory scale. The aim of this study was to report the performance of the typical commercial catalysts in total oxidation of model volatile organic compounds (ethanol, toluene, and dichloromethane) at laboratory scale and to describe their physicochemical properties.

2. Experimental

2.1. Catalysts

Commercial catalysts EnviCat® HHC-5557, EnviCat® VOC-5565, and EnviCat® VOC-1544 were purchased from Südchemie,

* Corresponding author. Tel.: +420 220 390 282; fax: +420 220 920 661.
E-mail address: topka@icpf.cas.cz (P. Topka).

0926-860X/$ – see front matter © 2012 Elsevier B.V. All rights reserved.
http://dx.doi.org/10.1016/j.apcata.2012.07.018

Germany. According to their product data sheets, EnviCat® VOC-5565 is intended for the oxidation of VOC, EnviCat® HHC-5557 is designed for the oxidation of chlorinated VOC, and EnviCat® VOC-1544 is recommended for the oxidation of oxygenated VOC. The catalysts in the form of spheres were crushed into a powder and then sieved. The particle size fraction 0.160–0.315 mm was employed in all experiments. The catalysts were denoted as Pt–Pd/Al (EnviCat® HHC-5557), Pt–Pd/Al–Ce (EnviCat® VOC-5565), and Cu–Mn/Al (EnviCat® VOC-1544).

2.2. Characterization

The catalysts were characterized by X-ray fluorescence (XRF), X-ray powder diffraction (XRD), field-emission scanning electron microscopy (FE-SEM), N_2 physisorption, temperature programmed reduction by hydrogen (H_2–TPR), and temperature programmed desorption of ammonia (NH_3–TPD).

Chemical analysis of catalysts was done using an ICP-AES analyzer and XP sequential WD-XRF spectrometer Thermo ARL 9400. In order to obtain the most reliable results, the content of Pt, Pd, Cu and Mn was determined using ICP-AES analysis, while the content of other elements was analyzed using XRF.

The X-ray powder diffraction data were collected on a PANalytical XíPert PRO diffractometer in Bragg-Brentano geometry with fixed slits using Co Kα radiation. The patterns were acquired in the diffraction angle range 20–90° (2θ) with a step size of 0.02° (2θ).

The field-emission scanning electron microscopy (FE-SEM) images were taken using JEOL JSM-7500f scanning electron microscope. The samples for FE-SEM measurements were prepared by the powder dispersal in ethanol and subsequent dropping of the solution onto a carbon grid or by depositing the powder sample on a graphite tape.

N_2 physisorption on catalyst powders (grain size 0.160–0.315 mm) was performed using Micromeritics ASAP 2020 instrument after drying at 105 °C under 1 Pa vacuum for 24 h. The adsorption–desorption isotherms of nitrogen at −196 °C were treated by the standard Brunauer–Emmett–Teller (BET) procedure to calculate the specific surface area S_{BET}. The surface area of mesopores S_{meso} and the volume of micropores V_{micro} were determined by the *t*-plot method. The pore-size distribution (pore radius 10^0–10^2 nm) was calculated from the desorption branch of the adsorption–desorption isotherm by the advanced Barrett–Joyner–Halenda (BJH) method [11,12]. The Lecloux–Pirard standard isotherm [13] was employed for the *t*-plot as well as for the pore-size distribution evaluation.

The temperature-programmed reduction (TPR) measurements of catalysts (0.025 g) were performed with a H_2/N_2 mixture (10 mol% H_2), flow rate 50 mL min^{-1} and linear temperature increase 20 °C min^{-1} up to 1000 °C. A change in H_2 concentration was detected with a catharometer. Reduction of the grained CuO (0.160–0.315 mm) was performed in each experiment to calculate the absolute values of hydrogen consumed during reduction.

The temperature-programmed desorption (TPD) measurements of NH_3 was carried out to examine acid properties of the catalysts surface. The measurements were accomplished with 0.05 g of a sample in the temperature range 20–1000 °C, with helium as a carrier gas and NH_3 as an adsorbing gas. Prior to the measurement, each sample was calcined in helium at 500 °C, then cooled to 30 °C and an excess of NH_3 (ten doses, 840 μl each) was applied on the sample. Then, the sample was flushed with helium for 1 h to remove physically adsorbed ammonia and after that heating rate of 20 °C min^{-1} was applied. A change in NH_3 concentration was detected by the mass spectrometer Omnistar 300 (Pfeiffer Vacuum). During the experiments the following mass contributions *m*/*z* were collected: 2-H_2, 18-H_2O, and 16-NH_3. The TPR and TPD experiments were evaluated using the OriginPro 7.5 software with an accuracy of ±5%.

2.3. Catalytic experiments

Total oxidation of toluene was carried out in a fixed-bed flow glass reactor (inner diameter 5 mm) in the temperature range from 50 °C to 400 °C (the furnace temperature was linearly increased with the rate of 3.5 °C min^{-1}). The catalyst (0.225 g of sieved grains with particle size of 0.160–0.315 mm) was examined at 71 m^3 kg^{-1} h^{-1} space velocity. Temperature was measured inside the reactor before and behind the catalyst bed and the average temperature was taken as catalyst temperature. The inlet concentration of toluene in the air was 1000 volume ppm. The catalysts were used as-received without any pretreatment. Before the experiment the catalytic bed was kept under the feed stream until the toluene outlet concentration became constant.

Reaction products were analyzed by a gas chromatograph Hewlett-Packard 6890 equipped with a FID detector and a capillary column (HP-5 19091 J-413, 30 m × 0.32 mm × 0.25 mm with 5% phenylmethyl silicone). Concentrations of CO and CO_2 were monitored using a Siemens Ultramat 23 infrared analyzer. Conversion of toluene *C* and selectivity to carbon dioxide *S* were calculated based on the material balance using Eqs. (1) and (2):

$$C = \frac{a^{in} - a}{a^{in}} \quad (1)$$

$$S = \frac{n(a^{in} - a/fM) - \sum n_i a_i / f_i M_i}{n(a^{in} - a/fM) - \sum (n_i - 1) a_i / f_i M_i} \quad (2)$$

where a^{in} is the GC peak area of toluene corresponding to its inlet concentration (4.1 g m^{-3}), *a* is the GC peak area of toluene, *n* is the number of carbon atoms in the molecule of toluene, *f* is the experimentally determined FID relative response factor of toluene (1.05), *M* is the molecular weight of toluene, n_i is the number of carbon atoms in the molecule of corresponding by-product, a_i is the GC peak area of corresponding by-product, f_i is the experimentally determined FID relative response factor of corresponding by-product (1.00 for ethylene), and M_i is the molecular weight of corresponding by-product. The accuracy of the conversion and selectivity determination was ±2%.

Temperatures T_{50} and T_{90} (the temperature at which 50 and 90% conversion of the examined MC was observed, respectively) were chosen as a measure of catalyst activity. The catalyst selectivity was evaluated as the selectivity to CO_2 at 95% conversion of the examined MC ($S_{CD,95}$). In order to eliminate the influence of CO_2 adsorption on the catalyst, the selectivity was computed from GC peak areas using the material balance according to Eq. (2); at 95% conversion, the presence of CO was not detected in any of the experiments.

Total oxidation of dichloromethane and ethanol was carried out in a fixed-bed flow quartz tubular reactor (inner diameter 8 mm) enabling also tests with chlorinated compounds [14]. The reactor operating under atmospheric pressure was located in a vertically situated ceramic tubular oven. Temperature was measured outside the reactor on its wall right before the catalyst bed.

The analysis of reaction products was performed on the Gasmet DX-4000 N FTIR analyzer, which is able to detect almost all gaseous compounds excluding noble gases and diatomic homonuclear compounds such as O_2, N_2, and Cl_2. The analyzer consists of a high temperature sample cell, a temperature controller, a Peltier cooled MCT-detector and signal processing electronics. It was calibrated to detect following chlorinated hydrocarbons: C_2Cl_4, C_2HCl_3, CH_3Cl, CH_2Cl_2, $CHCl_3$, $COCl_2$, HCl and following oxyderivatives of hydrocarbons: CO_2, CO, CH_3CHO, CH_2O, CH_3COOH, $CH_3COOC_2H_5$, CH_3OH,

Table 1
Chemical composition of catalysts in wt%.

	Pt–Pd/Al	Pt–Pd/Al–Ce	Cu–Mn/Al
Cu	–	–	3.34
Mn	–	–	5.44
Pt	0.13	0.05	–
Pd	0.11	0.05	–
CeO_2	0.02	6.45	0.03
MgO	0.19	–	0.16
CaO	0.06	0.04	0.06
Na_2O	0.27	0.12	0.06
K_2O	0.03	0.01	0.01
Cl	0.35	–	–
Al_2O_3	98.75	92.84	90.75

CH_3CH_2OH and C_2H_4. The measured spectra were analyzed with Calcmet for Windows analysis software.

The initial dichloromethane (DCM) or ethanol concentration was 1000 volume ppm in all tests (DCM ~3.79 g m^{-3}, ethanol ~2.05 g m^{-3}). The activity tests with DCM were performed in the presence of 1.5 wt% of water to ensure sufficient amount of hydrogen and thus improve the selectivity towards desired HCl [15–20]. Each test was carried out with 0.870 g of fresh catalyst (grain size 0.160–0.315 mm) without any pretreatment. The flow of the reaction mixture was 1.03 l min^{-1}, which corresponded to the space velocity of 71 m^3 kg^{-1} h^{-1}. The reaction temperature was linearly increased from 100 °C to 500 °C with heating rate 3.5 °C min^{-1} (DCM oxidation) or from 50 °C to 400 °C with the same heating rate (ethanol oxidation). The catalysts were used as-received without any pretreatment. Before the experiment the catalytic bed was kept under the feed stream until the ethanol or DCM outlet concentration became constant.

Temperatures T_{50} and T_{90} were chosen as a measure of catalyst activity. Selectivity to CO_2 at 95% ethanol conversion ($S_{CD,95}$) was calculated according to Eq. (3):

$$S_{CD,95} = \frac{n_{CD}}{n_{CD} + \sum n_i} \quad (3)$$

where n_{CD} is the molar amount of CO_2 and $\sum n_i$ is the sum of molar amounts of all other detected reaction products except H_2O. For DCM oxidation, the maximum HCl yield $Y_{HCl,max}$ and the HCl yield at 95% DCM conversion $Y_{HCl,95}$ were evaluated according to Eq. (4):

$$Y_{HCl} = \frac{c_{HCl}}{2c^{in}_{DCM}} \quad (4)$$

where Y_{HCl} is the HCl yield, c_{HCl} is the output concentration of HCl, and c^{in}_{DCM} is the input concentration of DCM (both concentrations are in volume ppm).

3. Results and discussion

3.1. Characterization of the catalysts

Chemical composition of catalysts determined by ICP-AES and XRF is summarized in Table 1. Two examined catalysts are based on Pt and Pd. The Pt–Pd/Al catalyst contains higher amount of Pt and Pd (0.13 and 0.11 wt%, respectively) than the Pt–Pd/Al–Ce catalyst (0.05 and 0.05 wt%, respectively). In the Pt–Pd/Al–Ce catalyst, Pt and Pd are deposited on a mixed support composed of Al_2O_3 (92.84 wt%) and CeO_2 (6.45 wt%), while the Pt–Pd/Al catalyst is supported on Al_2O_3 (98.75 wt%). In contrast to the catalysts containing noble metals, the third catalyst (Cu–Mn/Al) is based on Cu and Mn oxides supported over Al_2O_3. Amount of Cu and Mn oxides is significantly higher (8.78 wt%) than that of the noble metal catalysts. The catalysts also contain traces of alkali and alkali earth metal oxides (0.55 and 0.17 wt% for Pt–Pd/Al and Pt–Pd/Al–Ce catalysts, respectively, and 0.29 wt% for the Cu–Mn/Al catalyst). In the Pt–Pd/Al catalyst, 0.35 wt% of chlorine was detected, which is very likely coming from chloroplatinic acid used during the synthesis of the catalyst.

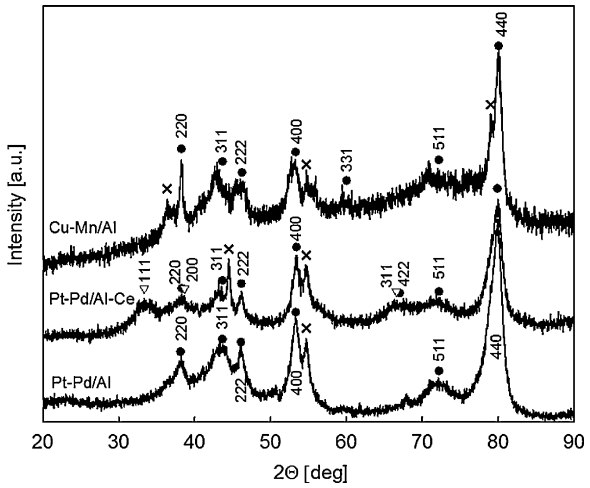

Fig. 1. X-ray diffraction patterns of Pt–Pd/Al, Pt–Pd/Al–Ce and Cu–Mn/Al (● γ-Al_2O_3/α-Al_2O_3, ▽ cubic CeO_2 (cerianite), × unidentified).

X-ray diffraction patterns of the catalysts measured using Co Kα radiation are shown in Fig. 1. Due to the unknown nature of alumina precursor(s) and the procedures and temperatures by which the alumina precursor(s) were treated to produce the final commercial catalysts it should be noted that the differentiation of alumina phases presented in the examined catalysts is very complex and might be extremely speculative. Based on the knowledge of maximum temperatures to which the catalysts can be used, i.e. 680 °C for the Pt–Pd/Al and Pt–Pd/Al–Ce catalysts and 500 °C for the Cu–Mn/Al catalyst, the γ-, η- and α-alumina were assumed for the identification. Because the cubic γ-alumina and η-alumina are hardly distinguishable, it cannot be surely concluded which of these two alumina phases exhibits higher symmetry of reflections. However, in all patterns the untypical split of (4 0 0) reflection, (3 1 1) reflection (in Pt–Pd/Al–Ce) and (2 2 0) and (4 4 0) reflections (in Cu–Mn/Al) can be seen. These features lead to the idea that (i) probably some amount of another type of alumina than γ and η is present in the catalysts and/or (ii) identified cubic alumina might be low-symmetric, e.g. due to strong hydroxylation. Snyder et al. [21] studied the transformation of boehmite and bayerite to γ-, η- and θ-alumina at elevated temperature. The split of all these reflections was observed for structural transformation to θ-alumina, however, they did not observed the coexistence of γ- and η- with θ-alumina. The split of (3 1 1) reflection can be also seen in corundum (α-alumina), but its other intense peaks are missing in the diffraction patterns of the Pt–Pd/Al–Ce catalyst. In the Pt–Pd/Al–Ce catalyst, the presence of another nanocrystalline phase – cubic CeO_2 (cerianite) – is confirmed by (1 1 1) reflection at $2\theta = 33.3°$. Other intense CeO_2 reflections (2 0 0 and 3 1 1) cannot be found because they are either not present or are overlapped by γ-lumina (2 2 0) and (4 2 2) reflections. The crystallite sizes of oxidic phases were not evaluated due to defects in alumina, which is far from the ideal crystal structure. Crystalline phases of Pt and Pd oxides were not found due to their low concentrations in both the Pt–Pd/Al and Pt–Pd/Al–Ce catalysts. Any crystalline phases of following Cu and/or Mn oxides were not identified: $CuMn_2O_4$, $CuMnO_2$, Cu_2O, CuO and Mn_3O_4. Cu and/or Mn oxides are either amorphous or their diffraction lines are overlapped by intense diffraction lines of aluminas.

Three selected FE-SEM images illustrate the morphology of the catalysts (Fig. 2). Fig. 2a (catalyst Pt–Pd/Al) shows irregular aggregates of a matter composed of primary fine and relatively uniform nanoparticles. Very similar nanoparticulate morphology can be seen also in Fig. 2b where the Pt–Pd/Al–Ce catalyst is presented.

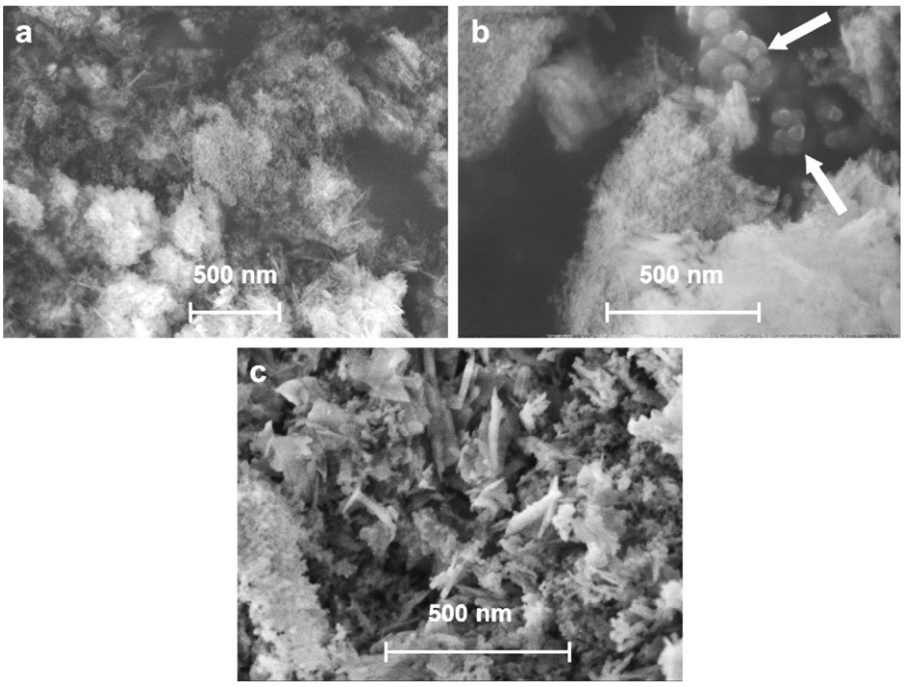

Fig. 2. FE-SEM images of: (a) Pt–Pd/Al; (b) Pt–Pd/Al–Ce and (c) Cu–Mn/Al.

In addition to the primary nanoparticles the larger nanoparticles with the size around 40–45 nm are also visible in this case. The FE-SEM image of the Cu–Mn/Al catalyst is shown in Fig. 2c. Here, the mixture of fine nanoparticles with irregular flakes can be seen. These flakes could be assigned either to Cu and Mn oxides or to a type of alumina which is not present in Pt–Pd/Al and Pt–Pd/Al–Ce catalysts.

N_2 physisorption was used to determine the textural parameters of the catalysts. The obtained results are summarized in Table 2. Although the use of classic (two-parameter) BET equation for the analysis of adsorption isotherms of microporous–mesoporous samples is not correct [22], the surface area S_{BET} is also included in Table 2 for comparison with literature data. The nitrogen adsorption–desorption isotherms recorded at −196 °C are depicted in Fig. 3a with the adsorbed amount, a, expressed as gas adsorbate volume per gram of adsorbent for all samples. Nitrogen isotherms of all catalysts are very similar and correspond to the combination of I and IV type isotherms according to IUPAC classification [23]. For all samples a small increase of adsorption amount for $x = p/p_0 \rightarrow 0$ is evident, which indicates the presence of

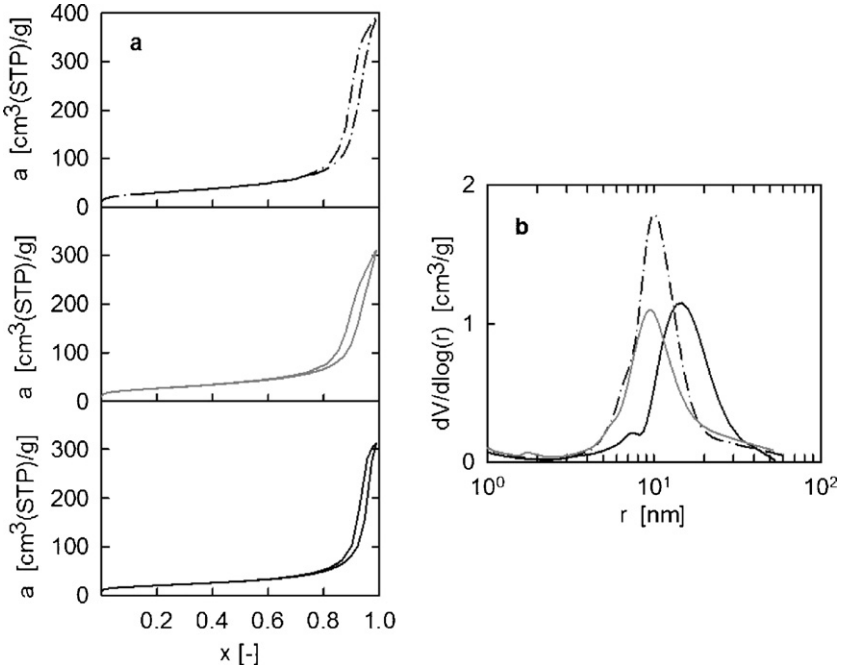

Fig. 3. (a) N_2 adsorption–desorption isotherms at −196 °C and (b) pore-size distributions evaluated from nitrogen physical adsorption of Pt–Pd/Al (dash-dot line), Pt–Pd/Al–Ce (gray line) and Cu–Mn/Al (black line).

Table 2
Textural properties of catalysts and their TPR and TPD characteristics.

Catalyst	S_{BET} ($m^2\ g^{-1}$)	S_{meso} ($m^2\ g^{-1}$)	V_{micro} ($mm_{liq}^3\ g^{-1}$)	V_p[a] ($mm_{liq}^3\ g^{-1}$)	H_2–TPR[b] (mmol g^{-1})	H_2–TPR[c] (mmol g^{-1})	NH_3–TPD[b] (mmol g^{-1})
Pt–Pd/Al	107	70	21	593	0.02	0.16	0.47
Pt–Pd/Al–Ce	96	60	20	464	0.18	0.75	0.17
Cu–Mn/Al	73	43	17	472	0.94	1.42	0.29

[a] Net pore volume (for $p/p_0 = 0.985$).
[b] Quantitative data in the temperature range from 25 °C to 500 °C.
[c] Quantitative data in the temperature range from 25 °C to 1000 °C.

micropores. A steep part of hysteresis loop (x between 0.80 and 0.985) points to the narrow mesopore-size distribution. Mesopore surface areas, S_{meso}, evaluated by the three-parameter BET equation [24] were relatively high (from 43 $m^2\ g^{-1}$ to 70 $m^2\ g^{-1}$); all catalysts also include a small and comparable portion of micropores. BET surface areas of all catalysts varied between 73 $m^2\ g^{-1}$ and 107 $m^2\ g^{-1}$. The pore-size distributions evaluated from the desorption curves of nitrogen physisorption isotherms are presented in Fig. 3b. Pt–Pd/Al and Pt–Pd/Al–Ce catalysts revealed the monodisperse pore structure with r_{max} of the main peak at 10 nm and 9 nm, respectively. The Cu–Mn/Al catalyst showed also monodisperse pore structure, however, with larger radius of mesopores (14 nm). It is obvious that the textural properties of the catalysts result from their composition.

The reducibility of the catalyst can be an important factor for the catalytic oxidation [25]. Moreover, it was shown that reducing the catalyst before testing can enhance its catalytic activity [26]. The reducibility of the investigated catalysts was examined by the temperature-programmed reduction using hydrogen as a reduction component. Fig. 4 demonstrates that practically all reducible compounds in the Cu–Mn/Al catalyst were completely reduced in the temperature range 25–400 °C with maximum of the reduction rate at 258 °C. This reduction peak comprises not only the reduction of CuO present in the catalyst but also reduction of Mn oxides, i.e., reduction of Mn^{4+} to Mn^{3+} and Mn^{3+} to Mn^{2+}. These findings correspond to the data obtained by Buciuman et al. [27] during TPR measurement of hopcalite ($CuMn_2O_4$) calcined at 550 °C, where the main reduction peak at 320 °C and shoulders at 260 and 380 °C were found. Reduction profiles of the catalysts containing noble metals (Pt–Pd/Al and Pt–Pd/Al–Ce) are more complex. Following reduction maxima can be found for the compounds of both noble metals in the literature: PtO, PtO_2 and $PtAl_2O_4$ supported on alumina are reduced at 58, 110, and 227 °C, respectively [28]; PdO is reduced at temperatures around 260 °C [29]. The TPR profile of the Pt–Pd/Al catalyst showed the distinct peak at 115 °C. It could be ascribed either to elimination of water physisorbed on the catalyst or reduction of PtO_2. In addition, two small reduction peaks at 376 and 488 °C can be recognized. As the catalyst does not comprise other reducible components than Pt and Pd oxides, both peaks must represent reduction of the Pt and Pd oxides present on the support in various particle sizes. In the TPR profile of the Pt–Pd/Al–Ce catalyst, three main reduction peaks can be recognized at 183, 438 and 560 °C together with a shoulder at 107 °C. The shoulder at 107 °C can be ascribed to the elimination of water physisorbed on the catalyst [30]. Reduction of both Pt oxide and surface CeO_2 particles, which are in close contact with Pt can proceed at 183 °C, as platinum promotes the reduction of ceria at low loadings [31]. The peak at 438 °C can be attributed to the reduction of surface oxygen of cerium oxide [32]. The peak at 560 °C is ascribed to the formation of nonstoichiometric Ce oxides; this peak was identified as the main peak in the TPR profiles of CeO_2–Al_2O_3 supports with different CeO_2 loading and calcined at 500 °C [31]. Reduction curves were integrated in the temperature range of 25–500 °C, potentially having relation to catalytic oxidation reaction, and the amounts of easily reducible components were calculated based on the calibration using CuO. Quantitative data are summarized in Table 2. The highest amount of hydrogen consumed in the temperature range 25–500 °C was found with Cu–Mn/Al catalyst (0.94 mmol g^{-1}), followed by Pt–Pd/Al–Ce catalyst (0.18 mmol g^{-1}). The lowest amount of reducible components showed the Pt–Pd/Al catalyst (0.02 mmol g^{-1}). The difference in hydrogen consumption between Pt–Pd/Al and Pt–Pd/Al–Ce catalyst, which contain similarly small amount of Pt + Pd (0.2 and 0.1 wt%, respectively), can be explained by the presence of relatively large amount of CeO_2 (6.45 wt%) in the latter catalyst.

TPD patterns of ammonia desorption from the examined catalysts are shown in Fig. 5. Desorption of ammonia proceeded in the temperature range of 25–450 °C only. It indicates that the catalysts do not comprise very strong acidic sites. A distinct desorption peak can be recognized at 98 °C with two shoulders at 166 and 292 °C with the Pt–Pd/Al catalyst. It means that the catalyst comprises acidic sites of different strength-low, medium and strong. In contrast, the Cu–Mn/Al catalyst shows a broad peak with maximum at 140 °C and a peak of medium strength, not clearly

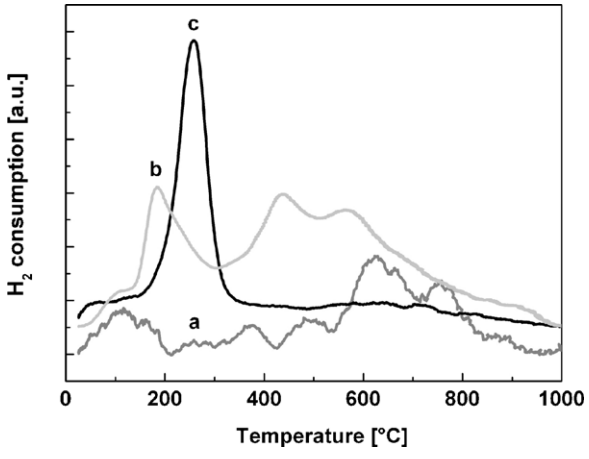

Fig. 4. H_2–TPR profiles of: (a) Pt–Pd/Al; (b) Pt–Pd/Al–Ce and (c) Cu–Mn/Al. For clarity, the profile of Cu–Mn/Al was divided by 5.

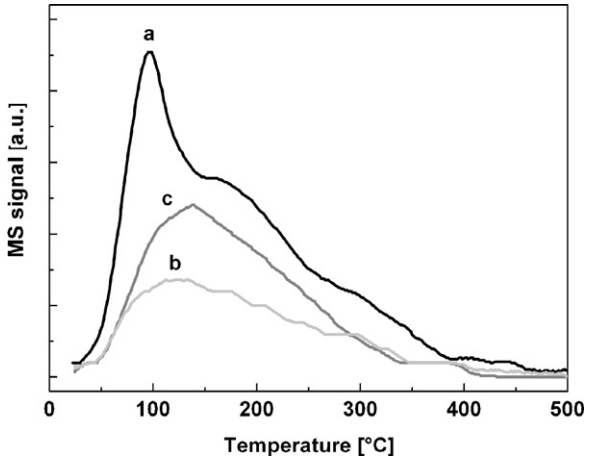

Fig. 5. NH_3–TPD profiles of: (a) Pt–Pd/Al; (b) Pt–Pd/Al–Ce and (c) Cu–Mn/Al.

distinguished. The lowest ammonia desorption peak was found with the Pt–Pd/Al–Ce catalyst (peak maxima at 127 and 295 °C). Lower acidity of the catalyst can be likely caused by the presence of ceria (6.45 wt%) in the alumina support together with lower concentration of noble metals in the catalyst. The highest amount of desorbed ammonia was observed with the Pt–Pd/Al catalyst followed by Cu–Mn/Al and Pt–Pd/Al–Ce catalysts (Table 2).

3.2. Catalytic tests

Results of dichloromethane oxidation over investigated catalysts are shown in Table 3. Comparison of T_{50} and T_{90} leads to the conclusion that the Pt–Pd/Al–Ce catalyst is the most active one (T_{50} = 409 °C) despite a lower content of Pt in comparison with the Pt–Pd/Al catalyst. The Cu–Mn/Al catalyst exhibited slightly lower catalytic activity – T_{50} was 416 °C. Surprisingly, the Pt–Pd/Al catalyst showed the lowest activity (T_{50} = 452 °C). This ranking in catalytic activity can be explained based on the data summarized in Table 2 and depicted in Figs. 4 and 5. It is known that in the oxidation of chlorinated methanes, the acidity of the catalysts is a key factor for their sufficient catalytic activity [20,33–36]. Concerning the noble metal catalysts, which are generally more suitable for chlorinated VOC oxidation, the Pt–Pd/Al–Ce catalyst exhibited lower acidity than Pt–Pd/Al (0.17 and 0.47 mmol g^{-1}, respectively; Table 2). On the other hand, Pt–Pd/Al–Ce showed significantly increased reducibility (0.18 mmol g^{-1}) in comparison with Pt–Pd/Al (0.02 mmol g^{-1}), although it contains lower amount of Pt and Pd. It is evident that this increase in reducibility can be ascribed to the addition of CeO_2; the reduction of Ce^{4+} to Ce^{3+} starts already around 180 °C with the maximum at 438 °C (Fig. 4). As the Pt–Pd/Al–Ce catalyst exhibited significantly higher activity in comparison with Pt–Pd/Al and the difference in reducibility between these two catalysts was much higher than the difference in acidity, it can be concluded that the reducibility of the catalyst may be also taken into account as an important characteristic that might correlate with catalytic activity in the oxidation of chlorinated compounds. This conclusion is supported by the superior activity of the Cu–Mn/Al catalyst in comparison with the Pt–Pd/Al catalyst. Assuming the same nature of the alumina support this difference in catalytic activity can be correlated with a relatively very high reducibility of the Cu–Mn/Al catalyst (0.94 mmol g^{-1}) due to the high amount of reducible Mn and Cu species.

In the oxidation of chlorinated VOC, the selectivity of the catalysts is at least as important as their activity due to possible formation of harmful chlorinated by-products (e.g. perchloroethylene, chloroform, trichloroethylene) that can be produced apart from chlorine and desired HCl [37,38]. From comparison of HCl yields at the temperature of 95% DCM conversion (Table 3) it is seen that the HCl yields achieved with Pt–Pd/Al–Ce and Cu–Mn/Al catalysts are comparable (72% and 73%, respectively). On the other hand, with the Pt–Pd/Al catalyst the 95% conversion was not achieved up to 500 °C and the value of $Y_{HCl,95}$ is therefore not available. The maximum HCl yield was decreasing in the order Pt–Pd/Al > Pt–Pd/Al–Ce > Cu–Mn/Al (Table 3).

Except HCl and CO_2 as main products, following by-products were found in the output stream when the 1.5 wt% of water was injected into the input stream: CO, CH_2O, and $CHCl_3$. The concentration profiles of desired HCl and CO_2 together with all detected by-products of DCM oxidation are shown in Fig. 6a–c. Over Pt–Pd based Pt–Pd/Al and Pt–Pd/Al–Ce catalysts, traces of CO (20 ppm and 10 ppm, respectively) and CH_2O (15 ppm and 5 ppm, respectively) were detected besides CO_2. No chlorinated intermediates were found. The Pt–Pd/Al–Ce catalyst exhibited better results than Pt–Pd/Al: a reaction temperature of 480 °C was sufficient for total DCM oxidation yielding CO_2, HCl and chlorine. When the concentration profiles shown in Fig. 6a and b are compared, it is visible that

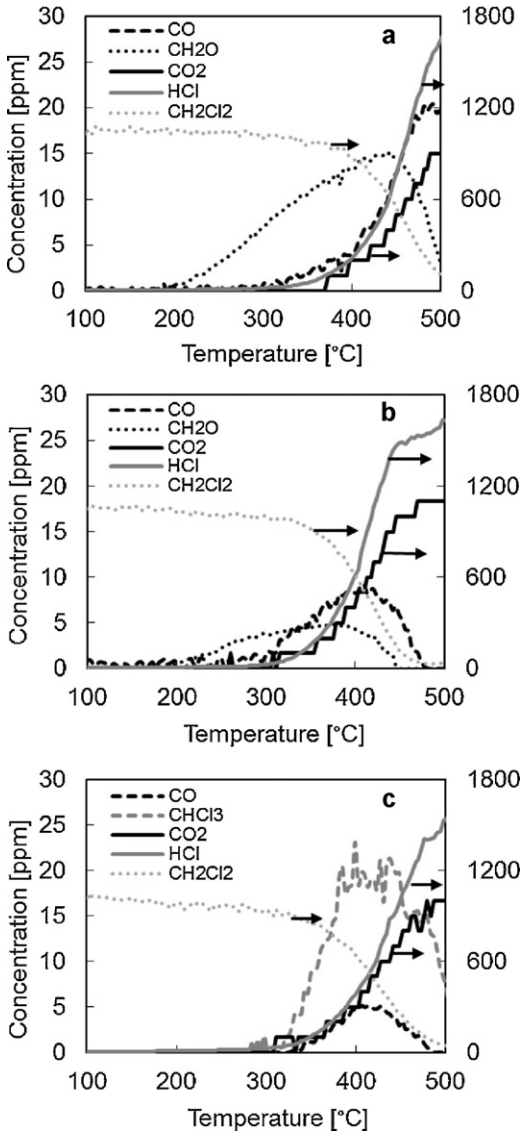

Fig. 6. Concentration profiles of dichloromethane and all detected products of dichloromethane oxidation: (a) Pt–Pd/Al; (b) Pt–Pd/Al–Ce and (c) Cu–Mn/Al. Dichloromethane concentration in air 1000 vpm, 1.5 wt% of water, space velocity 71 m^3 kg^{-1} h^{-1}, temperature ramp 3.5 °C min^{-1}; catalyst particle size 0.160–0.315 mm.

the presence of ceria in the Pt–Pd/Al–Ce catalyst enhanced its selectivity to CO_2. The Cu–Mn/Al catalyst produced traces of CO (5 ppm) and $CHCl_3$ (20 ppm) (Fig. 6c). Other possible harmful by-products such as perchloroethylene, trichloroethylene, methylchloride or phosgene were not detected with any of the investigated catalysts.

The laboratory tests with grained catalyst have shown that the Pt–Pd/Al–Ce catalyst is more active and also more selective to CO_2 than the Pt–Pd/Al catalyst. In the case of the Cu–Mn/Al catalyst, the selectivity to CO_2 was higher than that of the Pt–Pd/Al catalyst. However, undesirable harmful chlorinated by-product – chloroform – was formed. The selectivity of the Cu–Mn/Al catalyst corresponds to the observations of Miranda et al. [39] and Döbber et al. [40] who studied supported manganese oxides. Miranda et al. [39] investigated oxidation of trichloroethylene (TCE) over grained commercial Mn/Al_2O_3 catalyst. They observed the formation of undesired higher chlorinated by-products as tetrachlorethylene (PCE), tetrachloromethane (TTCM) or trichlormethane (TCM) mainly at lower temperatures. The amount of TTCM and TCM formed was decreased by the

Table 3
Activity and selectivity of catalysts in total oxidation of ethanol, toluene and dichloromethane.

Catalyst	Ethanol[a]			Toluene[a]			Dichloromethane[b]			
	T_{50} (°C)	T_{90} (°C)	$S_{CD,95}$ (%)	T_{50} (°C)	T_{90} (°C)	$S_{CD,95}$ (%)	T_{50} (°C)	T_{90} (°C)	$Y_{HCl,max}$ (%)	$Y_{HCl,95}$ (%)
Pt–Pd/Al	166	178	82	214	223	100	452	500	80	–
Pt–Pd/Al–Ce	180	212	78	270	285	100	409	452	77	72
Cu–Mn/Al	142	184	99	282	301	100	416	477	74	73

[a] Concentration in air 1000 vpm, space velocity 71 $m^3\ kg^{-1}\ h^{-1}$, temperature ramp 3.5 °C min^{-1}; catalyst particle size 0.160–0.315 mm.
[b] Concentration in air 1000 vpm, 1.5 wt% water, space velocity 71 $m^3\ kg^{-1}\ h^{-1}$, temperature ramp 3.5 °C min^{-1}; catalyst particle size 0.160–0.315 mm.

addition of water to the reaction mixture. On the other side, the presence of water decreased the stability of the Mn catalyst. Similarly, the higher chlorinated methanes were also detected as by-products of chloromethane oxidation over zirconia-supported manganese oxide by Döbber et al. [40]. Gu et al. [41] examined $CuMn/ZrO_2–TiO_2–Al_2O_3$ catalyst in DCM oxidation. They proved its high efficiency since a total DCM conversion was reached at 470 °C. $CHCl_3$ was the only intermediate with maximum concentration at 380 °C. This performance was ascribed to the highly dispersed $CuMnO_x$ phase. Moreover, the authors also found out that the addition of ZrO_2 improved the reducibility of the active phase. Vu et al. [42] investigated the 5 wt% $CuMnO_x/TiO_2$ catalyst in the oxidation of chlorobenzene (CB). They reported high catalyst activity, selectivity and long-term stability of this system, which was attributed to the formation of the $Mn_{1.6}Cu_{1.4}O_4$ spinel phase. However, the deactivation of the catalyst was observed and the formation of oxychlorinated copper and manganese species were presumed to be responsible to the catalyst partial deactivation.

Based on all these findings it is possible to summarize that supported Cu–Mn catalysts could be promising for the oxidation of chlorinated VOC due to relatively high catalytic activity and low production costs. However, the efficient form of active species has to be tailored depending on the type of oxidized compounds. The negative features of these types of catalysts seem to be a formation of by-products [39–41] and lower resistance against deactivation by chlorine [42]. On the other hand, the investigated Pt–Pd catalysts did not produce any harmful chlorinated intermediates even if their activity and selectivity to CO_2 and HCl was relatively low (the Pt–Pd/Al catalyst). For this reason the noble metal catalysts can be reasonably considered as more appropriate for Cl-VOC oxidation than the catalysts based on metal oxides, which was also concluded by Ojala et al. [43].

It should be noted that the results of catalytic test at laboratory scale can be affected by the form of catalysts (powders contrary to monoliths/pellets/spheres) and their preparation procedure [20,37]. For example, in ref. [20], where the original monolithic form of Pt–Pd catalysts (1:4 Pt–Pd ratio) supported on alumina and alumina-ceria was investigated, the catalytic activity exhibited inverse trend than in this study. Moreover, significantly different results of DCM oxidation were observed with two Pt–Pd/alumina catalysts of the same composition but provided by two different manufacturers [37].

Results of ethanol oxidation are summarized in Table 3 and Fig. 7a–f. The catalytic activity of the catalysts decreased in the order Cu–Mn/Al > Pt–Pd/Al > Pt–Pd/Al–Ce. This trend is also clearly visible from the temperature dependence of ethanol concentration for each catalyst (Fig. 7a, c and e). Comparison of selectivity to CO_2 at 95% ethanol conversion (Table 3) leads to the conclusion that the Cu–Mn/Al catalyst, in contrary to Pt–Pd catalysts, is the most selective one ($S_{CD,95}$ = 99%), while the Pt–Pd/Al and Pt–Pd/Al–Ce catalysts possess lower selectivity to CO_2 ($S_{CD,95}$ = 82% and 78%, respectively). CH_3CHO, CO and CH_2O were found with the Pt–Pd/Al–Ce (Fig. 7c and d) and Cu–Mn/Al catalysts (Fig. 7e and f), which corresponds to the well-accepted mechanism of ethanol oxidation [44]. The by-products detected during ethanol oxidation over the Pt–Pd/Al catalyst are shown in Fig. 7a and b. Apart from CH_3CHO (up to ~400 ppm), a significant amount of CH_3COOH (~100 ppm) and traces of CO (~5 ppm), CH_2O (~6 ppm) and ethylacetate (~3 ppm) were found. These by-products agree well with the suggested mechanism of ethanol oxidation over Pt-based catalysts [44]. Different performance of the investigated Pt–Pd catalysts is likely connected with higher Pt loading of the Pt–Pd/Al catalyst in comparison with the Pt–Pd/Al–Ce catalyst (0.24 versus 0.10 wt% Pt + Pd). A higher activity of the Pt–Pd/Al catalyst may be also linked to its different surface acid properties (a higher amount of acid centers) as illustrated by NH_3–TPD profiles (Fig. 5, Table 2).

Results of toluene total oxidation over examined catalysts are shown in Table 3 and the light-off curves are depicted in Fig. 8. The courses of the light-off curves indicate relatively complex behavior of the examined catalysts in toluene oxidation. The low-temperature step in toluene conversion observed between ~140 °C and 260 °C in the case of Cu-Mn/Al catalyst could be connected with chemisorption of toluene on the catalyst. Correctness of this assumption is supported by the comparison of toluene conversion with CO_2 evolution during the experiment. From Fig. 8 it is seen that increase in toluene conversion over Cu–Mn/Al catalyst between ~140 °C and ~260 °C is not accompanied by corresponding increase in CO_2 concentration. On the other hand, a very intense peak in CO_2 concentration is observed when the reaction temperature reaches ~275 °C. This peak likely arises from the oxidation of a large amount of toluene previously adsorbed on the catalyst surface. Therefore, the low-temperature step in toluene conversion can be ascribed to toluene chemisorption on the catalyst.

The activity of the catalysts decreased in the order Pt–Pd/Al > Pt–Pd/Al-Ce > Cu–Mn/Al (T_{90} was 223, 285, and 301 °C, respectively). Observed trend in catalytic activity is in agreement with the generally known fact that noble metal catalysts are more active in the total oxidation of aromatic VOC than the catalysts based on transition metal oxides [45]. On the other hand, the evident positive effect of the presence of ceria in alumina support on toluene oxidation was recently reported [46,47]. Del Angel et al. [46] and Abbasi et al. [47] found that the combustion temperature of toluene diminished as the content of the ceria in γ-alumina support increased. It was also shown that the ability of ceria to exchange oxygen due to the redox cycle $Ce^{4+} \leftrightarrow Ce^{3+}$ can be related to the improvement in toluene oxidation. The XPS study revealed that the population of the Ce^{4+} species increases with increasing Ce content in the catalyst. Then, the higher is the Ce^{4+}/Ce^{3+} ratio in the catalyst, the higher is the activity of the ceria–alumina catalyst in toluene oxidation [46]. In addition, it was confirmed that ceria–alumina can enhance the reduction of Pt-oxide species and their mutual interaction can be responsible for better performance of the catalyst in toluene oxidation as well [47]. According to the H_2–TPR study in this work, the positive effect of ceria on the reducibility of the catalyst was observed when Pt–Pd/Al–Ce and Pt–Pd/Al catalysts were compared. However, due to different Pt and especially Pd content in the catalysts, no clear correlation between performance of these catalysts in toluene oxidation and their reducibility could be made. The positive

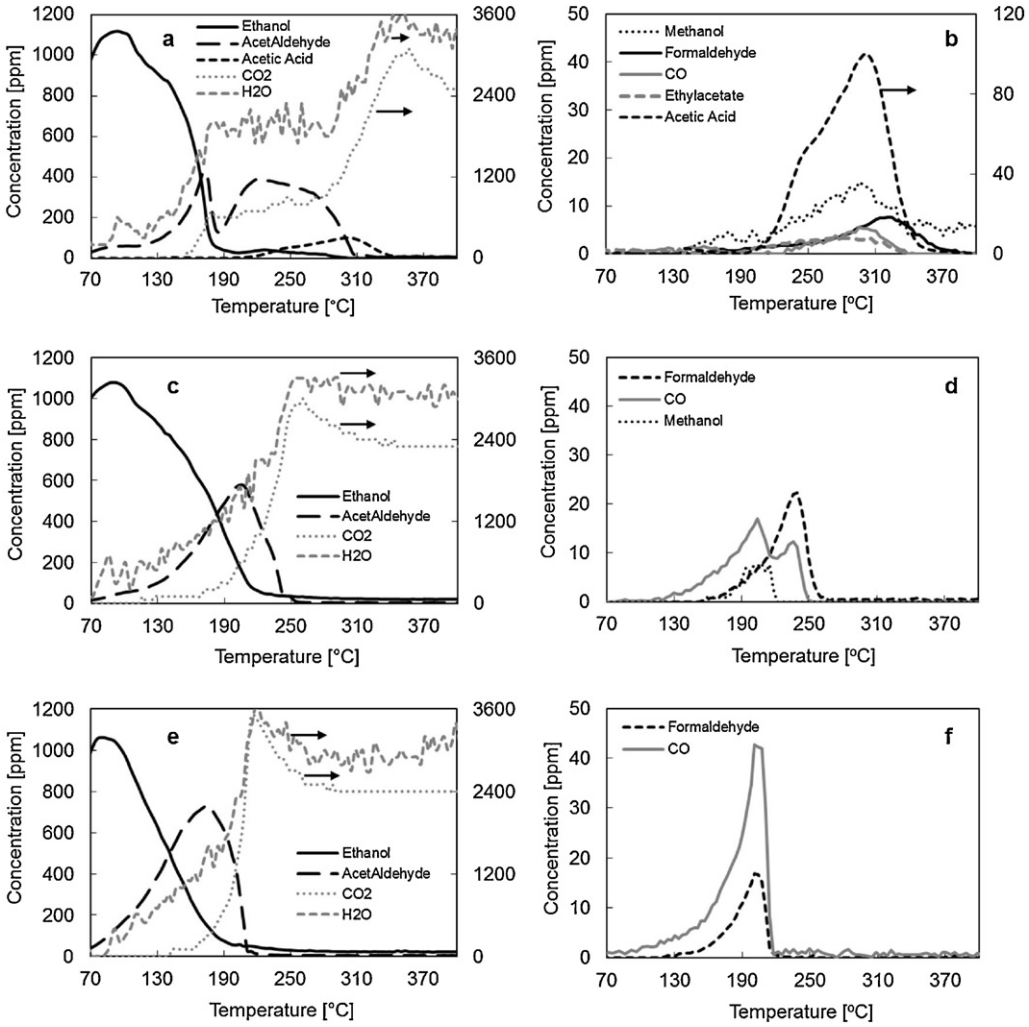

Fig. 7. Concentration profiles of ethanol and all detected products of ethanol oxidation: (a), (b) Pt–Pd/Al; (c), (d) Pt–Pd/Al–Ce and (e), (f) Cu–Mn/Al. Ethanol concentration in air 1000 vpm, space velocity 71 $m^3\ kg^{-1}\ h^{-1}$, temperature ramp 3.5 °C min^{-1}; catalyst particle size 0.160–0.315 mm.

effect of the increased Lewis acidity of γ-alumina-based catalyst in comparison with ceria-γ-alumina-based catalysts on the efficiency of toluene combustion was not confirmed [46]. However, in the noble metal catalysis the activity depends also on the noble metal loading [9,48]. Thus, remarkably lower noble metal loading in the Pt–Pd/Al–Ce catalyst (0.1 wt%) in comparison with Pt–Pd/Al catalyst (0.24 wt%) could be the main reason for higher T_{90} of the former catalyst and for the relatively large difference in T_{90} between them (62 °C).

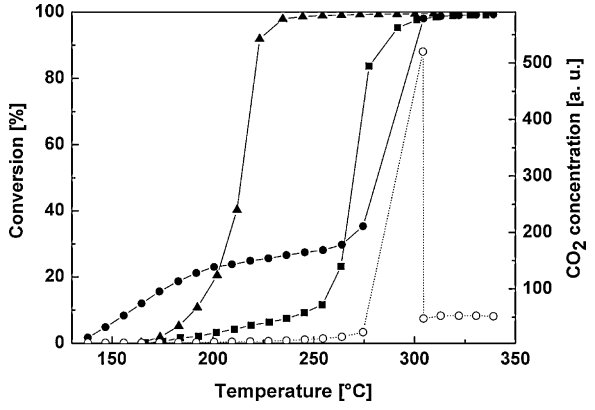

Fig. 8. Light-off curves of toluene total oxidation for Pt–Pd/Al (▲), Pt–Pd/Al–Ce (■) and Cu–Mn/Al (●) together with dependence of CO_2 concentration on reaction temperature for Cu–Mn/Al (○). Toluene concentration in air 1000 vpm, space velocity 71 $m^3\ kg^{-1}\ h^{-1}$, temperature ramp 3.5 °C min^{-1}; catalyst particle size 0.160–0.315 mm.

Also $CuMnO_x/\gamma\text{-}Al_2O_3$ catalysts have been studied and considered as very active and promising in toluene oxidation [49]. Li et al. [49] found out that bimetallic $CuMnO_x/\gamma\text{-}Al_2O_3$ catalysts with various molar ratios of Cu/Mn exhibit higher catalytic activity in toluene oxidation than monometallic $CuO_x/\gamma\text{-}Al_2O_3$ and $MnO_x/\gamma\text{-}Al_2O_3$ catalysts. It is mainly attributed to the formation of the $Cu_{1.5}Mn_{1.5}O_4$ spinel phase in the bimetallic catalysts. However, in the Cu–Mn/Al catalyst investigated in this work the presence of such structure, which could be responsible for the catalytic activity comparable to Pt–Pd/Al–Ce catalyst, can not be confirmed due to overlapping of alumina diffraction lines with that of Cu–Mn oxides in the X-ray diffraction pattern of the catalyst.

In VOC oxidation reactions, selectivity of catalysts to CO_2 is often even more important than their activity as some by-products formed during the oxidation can be more detrimental to the environment than the initial compounds. For example, benzene can be formed during toluene oxidation [50]. Generally, noble metal catalysts exhibit higher selectivity to CO_2 than metal oxide catalysts [43]. Investigated commercial catalysts revealed high selectivity in

the total oxidation of toluene ($S_{CD,95}$ = 100% for all catalysts) and no by-products were detected.

It may be interesting to compare the activity of commercial catalysts in the oxidation of model compounds investigated at laboratory scale with the information provided to industrial customers in catalyst data sheets. In our case, the Cu–Mn/Al catalyst was reported as "high performance catalyst for the oxidation of oxygenated VOC like alcohols, aldehydes, and ketones". Indeed, our results confirmed that this catalyst was the most active and selective one in the oxidation of ethanol. The results of dichloromethane oxidation were more complicated. The Pt–Pd/Al catalyst was described as "high performance catalyst for the total oxidation of halogenated (chlorinated) VOC". Nevertheless, the highest activity in dichloromethane oxidation was accomplished with Pt–Pd/Al–Ce, which was labeled as "high performance catalyst for the total oxidation of VOC". On the other hand, the highest HCl yield was reached with the Pt–Pd/Al catalyst (80%), followed by Pt–Pd/Al–Ce (77%). When we take into account that in oxidation of chlorinated VOC the selectivity (i.e. the HCl yield) is considered to be more important than activity [43], it can be concluded that these results are in agreement with the information provided by catalyst supplier. However, this is not the case of toluene oxidation. Here, the Pt–Pd/Al catalyst was the most active one, although it was recommended for the oxidation of chlorinated VOC. On the other hand, Pt–Pd/Al–Ce reported as "high performance catalyst for the total oxidation of VOC" was much less active (T_{50} was by 56 °C higher). The selectivity to CO_2 was 100% for all tested catalysts.

These results illustrate that the performance of commercial catalysts in laboratory scale tests may differ from that declared by catalyst supplier. This discrepancy may be connected with the fact that the catalysts, which were originally in the form of spheres, were crushed into a powder before the tests and therefore the physicochemical properties of the catalyst layer were changed. Thus, when industrial catalysts are crushed and employed in a powder form in laboratory scale tests (as e.g. in ref. [51]), such possible differences in catalytic performance should be taken into account.

4. Conclusions

The knowledge about catalytic and physicochemical properties of commercial catalysts can be helpful in developing new or improved catalysts at laboratory scale. In this study, three EnviCat® commercial catalysts (Pt–Pd/Al, Pt–Pd/Al–Ce and Cu–Mn/Al) designed for the total oxidation of the volatile organic compounds in air were characterized and employed in laboratory-scale testing using two different set-ups. The catalysts in the form of grains were tested in the total oxidation of three model compounds: ethanol, toluene, and dichloromethane. Two catalysts (Pt–Pd/Al and Pt–Pd/Al–Ce) contained Pt and Pd in a low concentration (less than 0.25 wt%), while the Cu–Mn/Al catalyst was based on Cu and Mn oxides in relatively high amount (8.78 wt%).

The reactivity of model VOC was decreasing in the order ethanol > toluene > dichloromethane. The most active catalysts were: the Cu–Mn/Al catalyst in ethanol oxidation, the Pt–Pd/Al catalyst in toluene oxidation and the Pt–Pd/Al–Ce catalyst in dichloromethane oxidation. The Cu–Mn/Al catalyst was also the most selective in ethanol oxidation: only CH_3CHO and traces of CO and CH_2O were detected. With Pt–Pd/Al and Pt–Pd/Al–Ce catalysts, traces of CH_3OH were also detected except common reaction by-products (CH_3CHO, CH_2O, CO, acetic acid and ethylacetate). It indicates the different oxidation mechanism over these two catalysts.

In toluene oxidation, the Pt–Pd/Al catalyst was the most active one, followed by Pt–Pd/Al–Ce. The Pt–Pd catalysts exhibited superior activity in comparison with Cu–Mn catalyst, while selectivity to CO_2 was 100% in all cases.

The most active in the oxidation of dichloromethane was the Pt–Pd/Al–Ce catalyst containing Pt and Pd (~1:1) supported on alumina–ceria. The superior activity of this catalyst may be attributed to the presence of CeO_2, which increased its ability to completely oxidize reaction by-products to CO_2 in the temperature range 400–500 °C. On the other hand, the highest HCl yield was achieved with Pt–Pd/Al, probably due to higher acidity of this catalyst in comparison with Pt–Pd/Al–Ce. No harmful chlorinated intermediates were detected with both Pt–Pd catalysts, while chloroform was produced over the Cu–Mn/Al catalyst.

It is necessary to state that the short-lasting laboratory tests could not cover other important features of commercial catalysts – their stability under reaction conditions and durability. The obtained results showed that the activity of commercial catalysts in laboratory scale tests can differ from that declared by catalyst supplier. A possible difference in catalytic performance at industrial and laboratory scale should be taken into account when industrial catalysts crushed into a powder form are used in laboratory scale tests. Nevertheless, comparison of the results obtained on new or improved oxidation catalysts with those found on commercial catalysts, though acquired only at laboratory scale, is always valuable.

Acknowledgements

The financial support of the Ministry of Industry and Trade of the Czech Republic (project No. FR-TI1/059) is gratefully acknowledged. The authors highly appreciate the kind support, fruitful discussions and help with experiments provided by Satu Pitkäaho, Dr. Satu Ojala and Prof. Riitta L. Keiski from the University of Oulu, Finland. The authors thank Filip Novotný from the Czech Technical University in Prague for FE-SEM images.

References

[1] R.G. Derwent, M.E. Jenkin, S.M. Saunders, M.J. Pilling, P.G. Simmonds, N.R. Passant, G.J. Dollard, P. Dumitrean, A. Kent, Atmos. Environ. 37 (2003) 1983–1991.
[2] M.M. Galloway, P.S. Chhabra, A.W.H. Chan, J.D. Surratt, R.C. Flagan, J.H. Seinfeld, F.N. Keutsch, Atmos. Chem. Phys. 9 (2009) 3331–3345.
[3] P. Hunter, S.T. Oyama, Control of Volatile Organic Compound Emissions, John Wiley, New York, 2000.
[4] Thematic Strategy on Air Pollution, Communication from the Commission to the Council and The European Parliament, Commission of the European Communities, COM (2005) 446 final, Brussels, 2005.
[5] F.I. Khan, A.K. Ghoshal, J. Loss Prev. Process Ind. 13 (2000) 527–545.
[6] A.C. Gluhoi, B.E. Nieuwenhuys, Catal. Today 119 (2007) 305–310.
[7] P.O. Larsson, A. Andersson, Appl. Catal. B 24 (2000) 175–192.
[8] J.J. Spivey, Ind. Eng. Chem. Res. 26 (1987) 2165–2180.
[9] L.F. Liotta, Appl. Catal. B 100 (2010) 403–412.
[10] W.B. Li, J.X. Wang, H. Gong, Catal. Today 148 (2009) 81–87.
[11] K.S.W. Sing, R.T. Williams, Adsorpt. Sci. Technol. 22 (2004) 773–782.
[12] L. Matějová, O. Šolcová, P. Schneider, Micropor. Mesopor. Mater. 107 (2008) 227–232.
[13] A. Lecloux, J.P. Pirard, J. Colloid Interf. Sci. 70 (1979) 265–281.
[14] S. Pitkäaho, L. Matějová, S. Ojala, J. Gaálová, R.L. Keiski, Appl. Catal. B 113-114 (2012) 150–159.
[15] K. Everaert, J. Baeyens, J. Hazard. Mater. 109 (2004) 113–139.
[16] R. López-Fonseca, J.I. Gutiérrez-Ortiz, J.R. González-Velasco, Catal. Commun. 5 (2004) 391–396.
[17] G. Sinquin, C. Petit, S. Libs, J.P. Hindermann, A. Kiennemann, Appl. Catal. B 27 (2000) 105–115.
[18] R. Lopez-Fonseca, S. Cibrian, J.I. Gutierrez-Ortiz, M.A. Gutierrez-Ortiz, J.R. Gonzalez-Velasco, AICHE J. 49 (2003) 496–504.
[19] J.R. Gonzalez-Velasco, A. Aranzabal, R. Lopez-Fonseca, R. Ferret, J.A. Gonzalez-Marcos, Appl. Catal. B 24 (2000) 33–43.
[20] S. Pitkaaho, S. Ojala, T. Maunula, A. Savimaki, T. Kinnunen, R.L. Keiski, Appl. Catal. B. 102 (2011) 395–403.
[21] R.S. Zhou, R.L. Snyder, Acta Crystallogr. Sect. B-Struct. Commun. 47 (1991) 617–630.
[22] P. Schneider, P. Hudec, O. Šolcová, Micropor. Mesopor. Mater. 115 (2008) 491–496.
[23] S.J. Gregg, K.S.W. Sing, Adsorption Surface Area and Porosity, Academic Press, New York, 1982.

[24] P. Schneider, Appl. Catal. A 129 (1995) 157.
[25] H.L. Tidahy, S. Siffert, J.F. Lamonier, R. Cousin, E.A. Zhilinskaya, A. Aboukais, B.L. Su, X. Canet, G. De Weireld, A. Frere, J.M. Giraudon, G. Leclercq, Appl. Catal. B 70 (2007) 377–383.
[26] T. Barakat, J.C. Rooke, H.L. Tidahy, M. Hosseini, R. Cousin, J.F. Lamonier, J.M. Giraudon, G. De Weireld, B.L. Su, S. Siffert, Chem. Sus. Chem. 4 (2011) 1420–1430.
[27] F.C. Buciuman, F. Pat, T. Hahn, Chem. Eng. Proc. 38 (1999) 563–569.
[28] Y.J. Huang, H.P. Wang, C.T. Yeh, S.H. Liu, B.C. Chang, Environ. Technol. 24 (2003) 377–382.
[29] K. Narui, K. Furuta, H. Yata, A. Nishida, Y. Kohtoku, T. Matsuzaki, Catal. Today 45 (1998) 173–178.
[30] R. Ramírez-López, L. Balderas-Tapia, I. Elizalde-Martinez, T. Viveros, Chem. Eng. Comm. 196 (2009) 1189–1197.
[31] A.C.S.F. Santos, S. Damyanova, G.N.R. Texeira, L.V. Mattos, F.B. Noronha, F.B. Passos, J.M.C. Bueno, Appl. Catal. A 290 (2005) 123–132.
[32] J.Z. Shyu, W.H. Weber, H.S. Gandhi, J. Phys. Chem. 92 (1998) 4964–4970.
[33] R.W. van den Brink, P. Mulder, R. Louw, G. Sinquin, C. Petit, J.P. Hindermann, J. Catal. 180 (1998) 153–160.
[34] H. Windawi, Z.C. Zhang, Catal. Today 30 (1996) 99–105.
[35] B. Ramachandran, H.L. Greene, S. Chatterjee, Appl. Catal. B 8 (1996) 157–182.
[36] R. Lopez-Fonseca, J.I. Gutierrez-Ortiz, J.L. Ayastui, M.A. Gutierrez-Ortiz, J.R. Gonzalez-Velasco, Appl. Catal. B 45 (2003) 13–21.
[37] J. Corella, J.M. Toledo, A.M. Padilla, Appl. Catal. B 27 (2000) 243–256.
[38] A. Koyer-Golkowska, A. Musialik-Piotrowska, J.D. Rutkowski, Catal. Today 90 (2004) 133–138.
[39] B. Miranda, E. Diaz, S. Ordonez, A. Vega, F.V. Diez, Chemosphere 66 (2007) 1706–1715.
[40] D. Dobber, D. Kiessling, W. Schmitz, G. Wendt, Appl. Catal. B 52 (2004) 135–143.
[41] Y. Gu, Y. Yang, Y. Qiu, K. Sun, X. Xu, Catal. Commun. 12 (2010) 277–281.
[42] V.H. Vu, J. Belkouch, A. Ould-Dris, B. Taouk, J. Hazard. Mater. 169 (2009) 758–765.
[43] S. Ojala, S. Pitkäaho, T. Laitinen, N. Niskala Koivikko, R. Brahmi, J. Gaálová, L. Matejova, A. Kucherov, S. Päivärinta, C. Hirschmann, T. Nevanperä, M. Riihimäki, M. Pirilä, R.L. Keiski, Top. Catal. 54 (2011) 1224–1256.
[44] A. Musialik-Piotrowska, K. Syczewska, Catal. Today 59 (2000) 269–278.
[45] P. Papaefthimiou, T. Ioannides, X.E. Verykios, Appl. Catal. B 13 (1997) 175–184.
[46] G. Del Angel, J.M. Padilla, I. Cuauhtémoc, J. Navareete, J. Mol. Catal. A 281 (2008) 173–178.
[47] Z. Abbasi, M. Haghighi, E. Fatehifar, S. Saedy, J. Hazard. Mater. 186 (2011) 1445–1454.
[48] S.F. Tahir, C.A. Koh, Chemosphere 38 (1999) 2109.
[49] X. Li, L. Wang, Q. Xia, Z. Liu, Z. Li, Catal. Commun. 14 (2001) 15–19.
[50] M.J. Patterson, D.E. Angove, N.W. Cant, P.F. Nelson, Appl. Catal. B 20 (1999) 123–131.
[51] E. Finocchio, M. Baldi, G. Busca, C. Pistarino, G. Romezzano, F. Bregani, G.P. Toledo, Catal. Today 59 (2000) 261–268.